(12) **LEVEL** $\overline{III}$

AD-E430612

AD

CONTRACT REPORT ARBRL-CR-00450

SABOT DESIGN OPTIMIZATION

Prepared by

Avco Systems Division
201 Lowell Street
Wilmington, MA 01887

March 1981

US ARMY ARMAMENT RESEARCH AND DEVELOPMENT COMMAND
BALLISTIC RESEARCH LABORATORY
ABERDEEN PROVING GROUND, MARYLAND

Approved for public release; distribution unlimited.

81 5 29 04

The findings in this report are not to be construed as
an official Department of the Army position, unless
so designated by other authorized documents.

The use of trade names or manufacturers' names in this report
does not constitute indorsement of any commercial product.

REPORT DOCUMENTATION PAGE		READ INSTRUCTIONS BEFORE COMPLETING FORM
1. REPORT NUMBER CONTRACT REPORT ARBRL-CR-00450	2. GOVT ACCESSION NO. AD-A100264	3. RECIPIENT'S CATALOG NUMBER
4. TITLE (and Subtitle) Sabot Design Optimization		5. TYPE OF REPORT & PERIOD COVERED Final
		6. PERFORMING ORG. REPORT NUMBER AVSD-0451-80-RR
7. AUTHOR(s) David Siegelman and Johnson Wang		8. CONTRACT OR GRANT NUMBER(s) DAAK11-77-C-0080
9. PERFORMING ORGANIZATION NAME AND ADDRESS Avco Systems Division 201 Lowell Street Wilmington, Massachusetts 01887		10. PROGRAM ELEMENT, PROJECT, TASK AREA & WORK UNIT NUMBERS
11. CONTROLLING OFFICE NAME AND ADDRESS US Army Armament Research & Development Command US Army Ballistic Research Laboratory (DRDAR-BL) Aberdeen Proving Ground, MD 21005		12. REPORT DATE MARCH 1981
		13. NUMBER OF PAGES 33
14. MONITORING AGENCY NAME & ADDRESS(if different from Controlling Office)		15. SECURITY CLASS. (of this report) Unclassified
		15a. DECLASSIFICATION/DOWNGRADING SCHEDULE

16. DISTRIBUTION STATEMENT (of this Report)

Approved for public release; distribution unlimited.

17. DISTRIBUTION STATEMENT (of the abstract entered in Block 20, if different from Report)

18. SUPPLEMENTARY NOTES

19. KEY WORDS (Continue on reverse side if necessary and identify by block number)
Sabot Discard
Design Optimization

20. ABSTRACT (Continue on reverse side if necessary and identify by block number)

An engineering analysis procedure which describes the sabot discard process for gun-launched projectiles has been employed to perform a sabot design optimization study. This analysis tool models the complex interaction flow field which develops about the projectile/sabot package by use of local shock/expansion procedures. Sabot design optimization was achieved based upon a figure of merit related to the pitching moment produced on the projectile during the removal process. A second constraint was also imposed to preclude

DD FORM 1473 EDITION OF 1 NOV 65 IS OBSOLETE

sabot contact with the projectile stabilizing fins during the discard. It was found that the front scoop/bore-rider size and axial location must be selected to provide an initial lateral motion with small rotation. This minimizes dispersive moments due to mechanical contact and helps provide fin clearance. This initial lateral motion phase must be followed by rapid pitch-up and deceleration in order to minimize the duration of the interaction process. The use of a novel winged sabot concept was found to show promise for providing such controllable sabot discard maneuvers.

FOREWORD

This study was conducted by Avco Systems Division for the U. S. Army Ballistic Research Laboratories under Contract No. DAAK11-77-C-0080. Technical Monitor for BRL was Dr. Edward M. Schmidt. Program Manager for Avco Systems Division was Dr. David Siegelman.

Accession For	✔
NTIS GRA&I	✔
DTIC TAB	☐
Unannounced	☐
Justification	
By	
Distribution/	
Availability Codes	
	Avail and/or
Dist	Special
A	

SUMMARY

An engineering analysis procedure which describes the sabot discard process for gun-launched projectiles has been employed to perform a sabot design optimization study. This analysis tool models the complex interaction flow field which develops about the projectile/sabot package by use of local shock/expansion procedures. Sabot design optimization was achieved based upon a figure of merit related to the pitching moment produced on the projectile during the removal process. A second constraint was also imposed to preclude sabot contact with the projectile stabilizing fins during the discard. It was found that the front scoop/bore-rider size and axial location must be selected to provide an initial lateral motion with small rotation. This minimizes dispersive moments due to mechanical contact and helps provide fin clearance. This initial lateral motion phase must be followed by rapid pitch-up and deceleration in order to minimize the duration of the interaction process. The use of a novel winged sabot concept was found to show promise for providing such controllable sabot discard maneuvers.

TABLE OF CONTENTS

ILLUSTRATIONS

LIST OF SYMBOLS

I_m The absolute value of the perturbing pitching moment impulse produced by a sabot segment

M Mach number

M_{pa} Pitching moment on the projectile due to sabot/projectile aerodynamic interaction

M_{pm} Pitching moment on the projectile due to sabot/projectile mechanical interaction

P Pressure

t_o Time duration of the sabot/projectile interaction

α Sabot pitch angle

R Nose radius

$Reff$ Effective nose radius

$X_{C.G.}, Y_{C.G.}$ Sabot center of gravity coordinates with respect to a frame of reference fixed on projectile

X_{TL}, Y_{TL} Sabot trailing edge coordinates with respect to a frame of reference fixed on projectile

Y_{st} Stagnation location

Subscripts

∞ Free stream condition

1 Background level on sabot underside

2 Value downstream of shock wave

NS static value downstream of normal shock wave

t Stagnation value downstream of normal shock wave

1.0 INTRODUCTION

The trajectory of a gun-launched projectile can be adversely affected by disturbances in the vicinity of the muzzle. In particular, projectiles launched with the aid of a sabot can be subjected to asymmetric forces and moments associated with the sabot discard process which could be significant contributors to dispersion. Recently, an engineering analysis was developed which describes sabot discard dynamics and the resultant loadings on the projectile, in order to provide a tool for assessing the influence of sabot, projectile and launch parameters upon projectile disturbances imparted in the vicinity of the muzzle.[1]

Aerodynamic interaction was found to be the key element of the overall system representation, as the sabot separation process was initially dominated by interactive aerodynamic effects. In order to better understand the nature of this interaction flow field, which develops when the projectile and sabot petal are in close proximity, BRL subsequently conducted a detailed wind tunnel test program at the NASA Langley test facility.[2-3] The experimental data indicated that individual compression wave intersections and reflections were clearly present within the annular flow passage. Based upon these findings an integrated flow element approach utilizing local shock/expansion procedures was developed and incorporated into the sabot discard dynamic motion code.[4-5] Comparisons between both measured wind tunnel pressure distributions and motions from actual firings of discarding sabot ammunition showed reasonable agreement with predictions from the shock/expansion theory code.

In the present work, this available treatment has been suitably extended and utilized to perform a sabot design optimization study aimed at defining sabot configurations which produce minimum dispersive pitching moments upon the projectile during the discard process. Design practices resulting in optimal sabot configurations have also been identified as outgrowth of this activity.

2.0 ANALYTIC MODEL

The dynamic motion model utilizes an inertial coordinate
system fixed at the projectile mass center. Sabot angular
orientations and translations are measured using body fixed axes
with origins at the sabot petal mass centers. Twelve degrees
of freedom are allowed for each of the four sabot segments
considered. In-bore effects such as spin, elastic decompression
and tip-off can be included by specification of appropriate initial
motion rates. Mechanical interaction is treated using a large
stiffness elastic body model with equal and opposite radial
reaction forces applied to both the sabot segment and projectile.
Details are provided in Reference 1.

Details of the interaction flow field model are given in
References 4 - 5. Figure 1A presents a summary overview which
highlights essentially all of the local flow elements previously
used to describe the overall surface pressure/aerodynamic force
behavior. The key features involve impingement of the sabot bow
shock upon the projectile surface resulting in a shock-reflection
process with attendant upstream boundary layer separation. The
reflected shock then impinges upon the sabot petal underside creat-
ing another separated zone of elevated pressure. Finally, under
certain conditions of (high) sabot petal incidence and small
sabot trailing edge displacement, an outlet region throttling
process is present. Based on the experimental data, axial pressure
variations on the sabot segment lateral edges are taken equal to
the sabot underside distribution.*

The previous flow model treated configurations having a
relatively simple conical scoop geometry. In order to adequately
treat the more complicated ramp/bore-rider configurations of current
practical concern, it was necessary to extend the flow element
model as shown in Figure 1B. The basic features of the up-dated
model are summarized below.

----

*Note that the present flow models are only strictly applicable
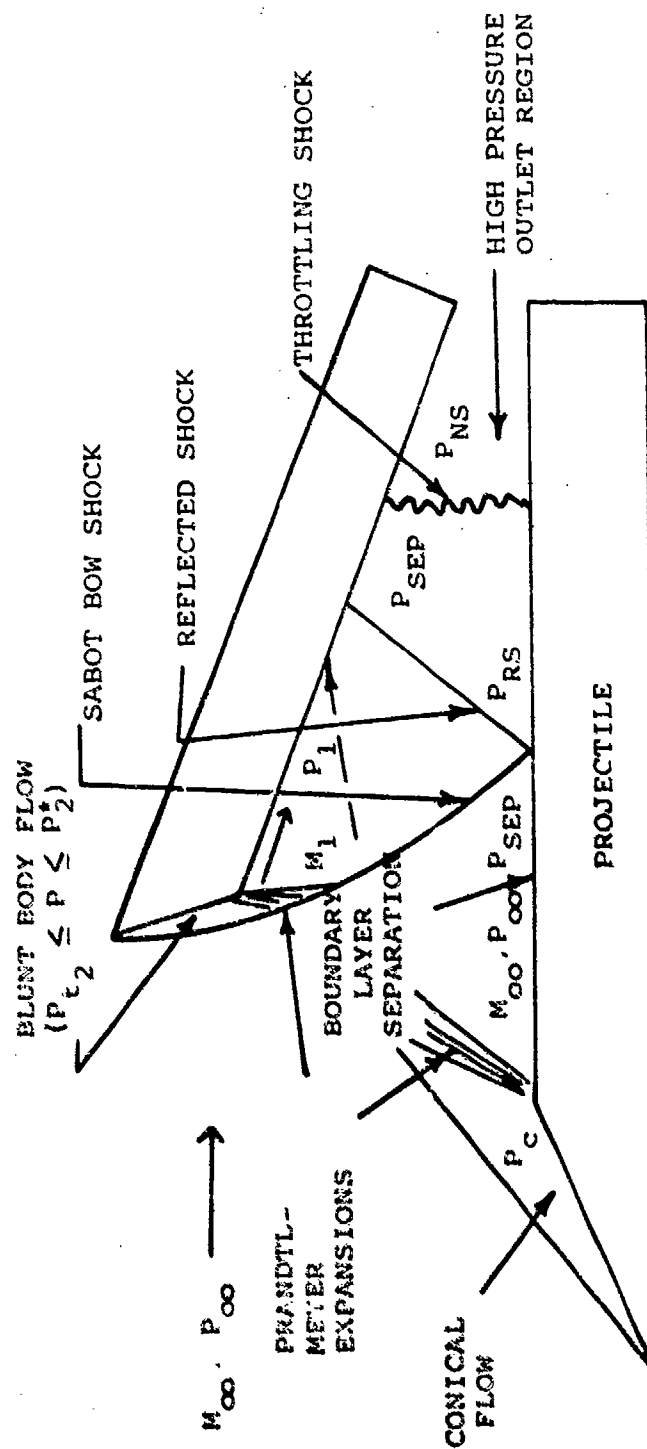to symmetric discards.

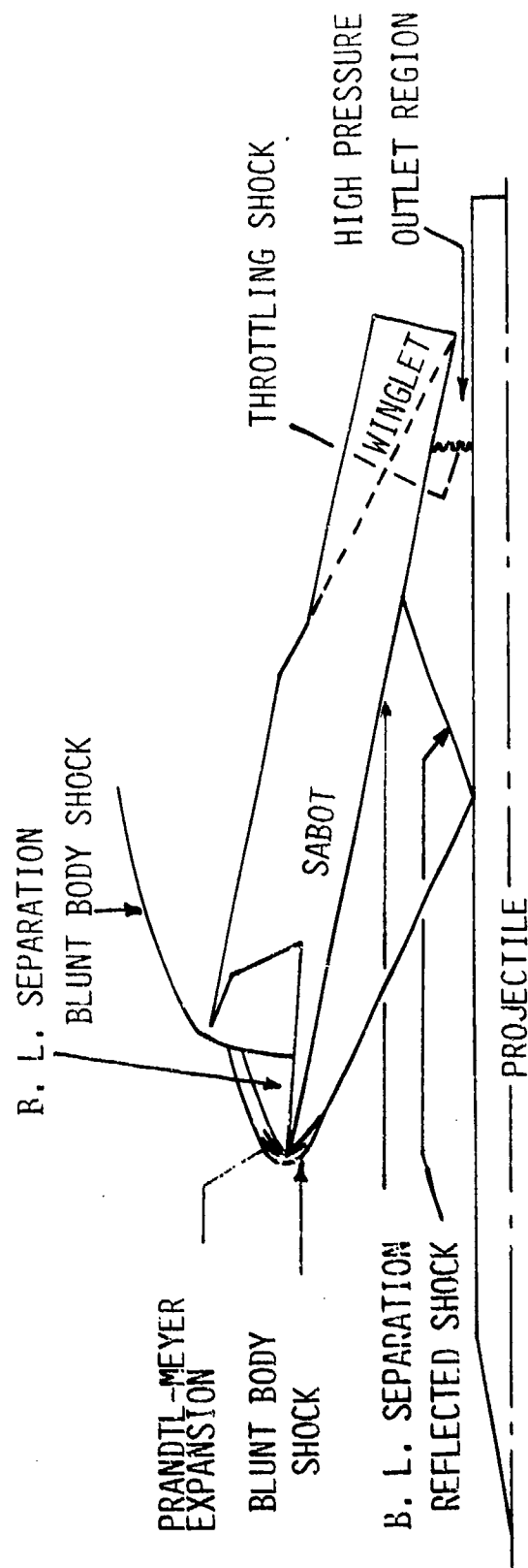FIGURE 1A - OVERVIEW OF PREVIOUS FLOW FIELD MODEL

FIG. 1B - OVERVIEW OF CURRENT FLOW FIELD MODEL

(1) Geometry - Three linear segments are now used to represent the front scoop/bore-rider geometric configuration.

(2) Aerodynamic Model - The separation bubble of the scoop bore-rider configuration is modeled as an equivalent flat face obstacle. The work of Katzen and Kaatari[6] is used to position the "stagnation point" at incidence:*

$$Y_{ST}/R = 3.03\alpha - 2.776\alpha^2 + .777\alpha^3 \qquad (1)$$

A comparison of this equation with the experimental data of Reference 6 is shown in Figure 2A. This work,[6] along with the higher Mach number information of Bolson and Curtiss,[7] was used to construct the pressure distribution on the scoop vertical surfaces. A sample angle of attack pressure distribution is shown in Figure 2B for a flight Mach number of 2.4 and an angle of attack of 20°.

Two subcases were considered in order to complete the scoop/ bore-rider flow model. For case one the shock layer thickness[7] in front of th flat obstacle is sufficient to contain the entire lower ramp projection. In this case the sabot thickness is used to characterize the shock wave length scale, as described in the previous work.[4] In case two the lower ramp projection extends forward of the scoop shock layer, as illustrated in Figure 1B. In this case the underside sabot bow shock length scale is characterized by the hydraulic radius of the forward ramp lip. This procedure was verified by comparison to available sabot dis- card photographs such as those shown in Figure 3A. As will be discussed in Section 4.4, configurations providing such a ramp extension are preferred because the sabot underside bow shock will attenuate quickly and provide less interactive aerodynamic force on the projectile.

Also, in case two an additional separation zone on the upper surface of the forward ramp extension is considered (see Figure 1B). The separation pressure in this zone is computed exactly as (and is equal to) that on the sabot underside.[4-5]

---

* Note α is measured in radians in this expression.

FIG. 2A - STAGNATION POINT LOCATION AS A FUNCTION OF INCIDENCE
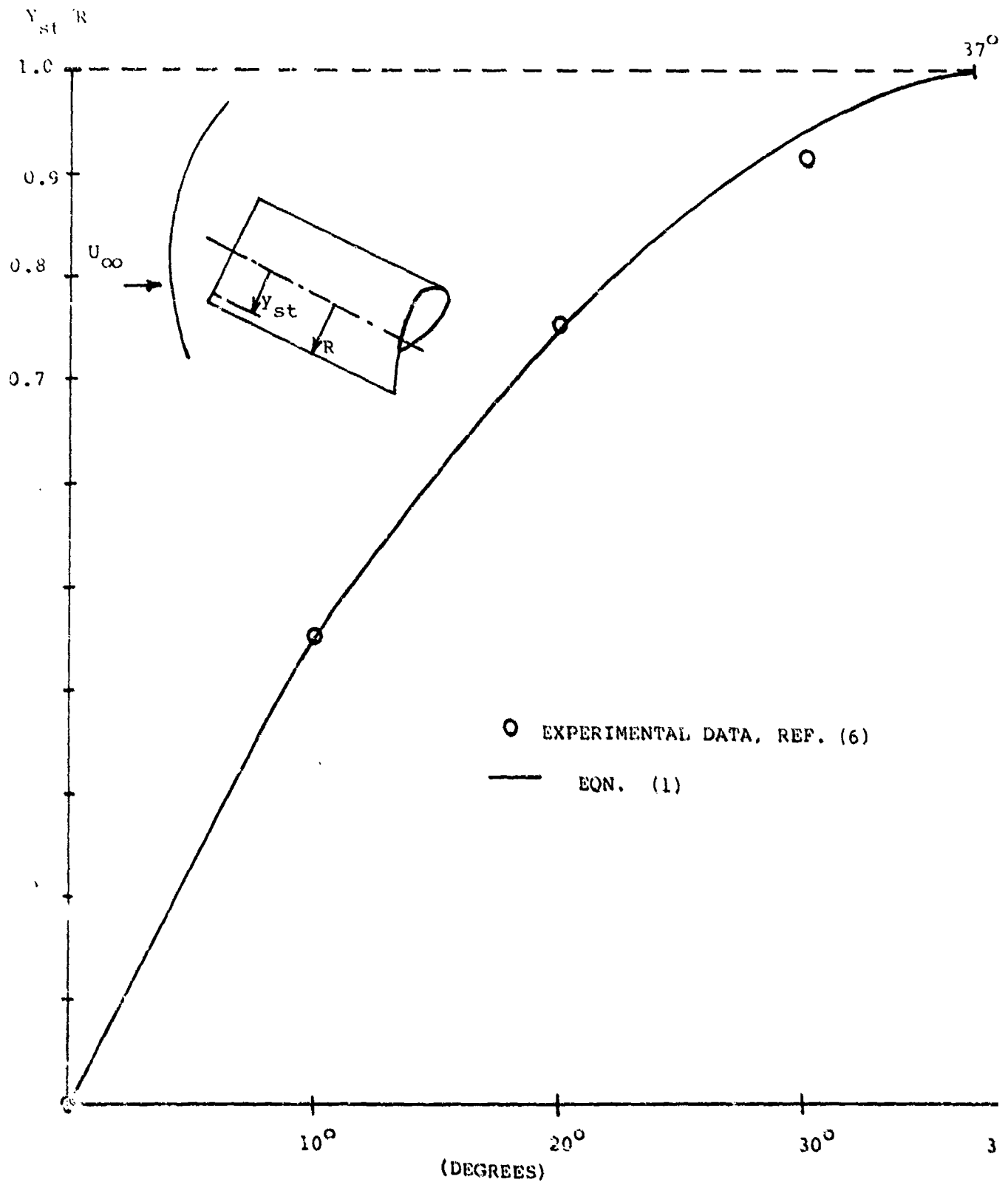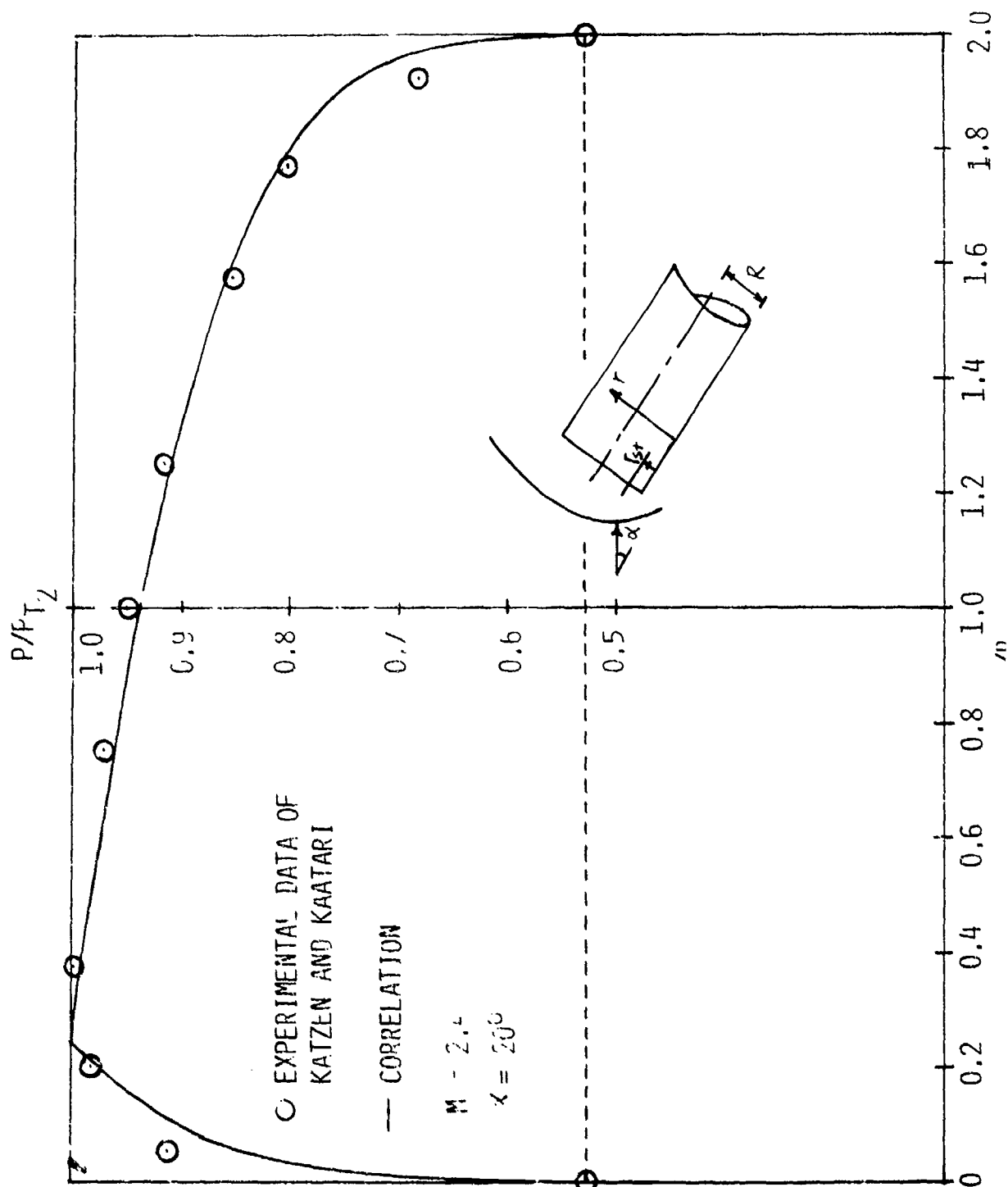
FIG. 2B – PRESSURE DISTRIBUTION ON A FLAT FACED BODY

P/P_{T_2}

○ EXPERIMENTAL DATA OF
   KATZEN AND KAATARI

— CORRELATION

$M = 2.4$
$\alpha = 20°$

That is, the background pressures and Mach numbers on both the upper surface of the ramp extension and the sabot underside are computed by a Prandtl Meyer expansion from the tip edge sonic point through a turn angle equal to the maximum deflection angle for an attached shock configuration. This turn angle is about 40° for a Mach 4.5 flow. This procedure was developed by use of the downstream sidewall surface pressure data given in Reference 7. Separation zone pressures were then computed using the turbulent separation data[8] previously discussed.[4-5]

One additional feature of the forward scoop model up-date needs mention. The previous work[4-5] located the sabot underside pressure rise region by use of a simple geometric procedure. It was noted that a more rigorous procedure would require use of the estimated sabot bow shock shape. This more rigorous method has now been incorporated into the flow field description procedure.

(3) Winglet Force Model - Aft mounted sabot winglets can be provided by extension of the sabot segment lateral edges. This is made possible by the radial taper present in double ramp sabot designs aft of the obturator ring. The pressures on such extended lateral surfaces were once again taken equal to the sabot underside pressures, based on the experimental data of References 2-3. As with all other sabot surfaces, Newtonian pressures are used whenever they exceed those predicted from the interaction model.[4-5]

(4) Pivot Rings - Pivot rings are circumferential bands placed around the projectile which butt up against the rear end of the sabot petals and prevent axial motion. They are intended to keep the sabot segments from impacting upon the projectile fins during discard. The presence of such pivot rings was treated using the available elastic body model. A horizontal mechanical force was applied to both the sabot segment and projectile (in the opposite direction, of course) until the sabot trailing edge lifts clear of the pivot ring height.

3.0 MODEL VALIDATION

Prior to conducting the sabot design optimization studies, it was clearly necessary to perform validation calculations to verify that the up-dated engineering model was sufficiently accurate to provide worthwhile design guidelines. Test data taken from actual firings of the 120 mm XM829 short wheel base design[9] (with pivot rings present) were used for this purpose. Figure 3 presents a comparison of analytical results with measured data. Photographs of the actual discard are shown in Figure 3A which compare extremely well with the predicted discard trajectories shown in Figure 3B. It was found in performing this comparison that corrections were required in order to achieve complete agreement between measured and code predicted axial locations of the sabot trailing edge. This problem arose because the code neglects projectile slowdown. It was found, however, that due to the presence of the pivot ring a force of about 1800 lbs. is transmitted to the projectile, resulting in a slowdown of about 43 ft/sec. This translated into an axial position shift of about 0.5 inch with regard to the sabot trailing edge. Furthermore, such findings also indicate that pivot rings should be avoided wherever possible in order to achieve optimum performance.

FIGURE 3A - 120 MM XM829 SHORT WHEEL BASE SABOT DISCARD WITH PIVOT RING

DISTANCE FROM MUZZLE   (Z) = 14 FT.

(Z) = 34 FT.

(Z) = 29 FT.

Z (FT)	PITCHING ANGLE (DEG.)		SABOT TAIL LOCATION (FT.)			
	COMPUTED	X-RAY	COMPUTED		X-RAY	
			$-X_{TL}$	Y_{TL}	$-X_{TL}$	Y_{TL}
14.0	4.5°	5.5°	0.0044	0.0411	--	--
29.0	25.3°	25.0°	0.067	0.1411	0.051	0.128
34.0	35.8°	33°	0.131	0.2067	0.120	0.2034

X_{TL} VALUES SHOWN IN FIGURE HAVE NOT BEEN CORRECTED FOR PROJECTILE SLOWDOWN

-11-
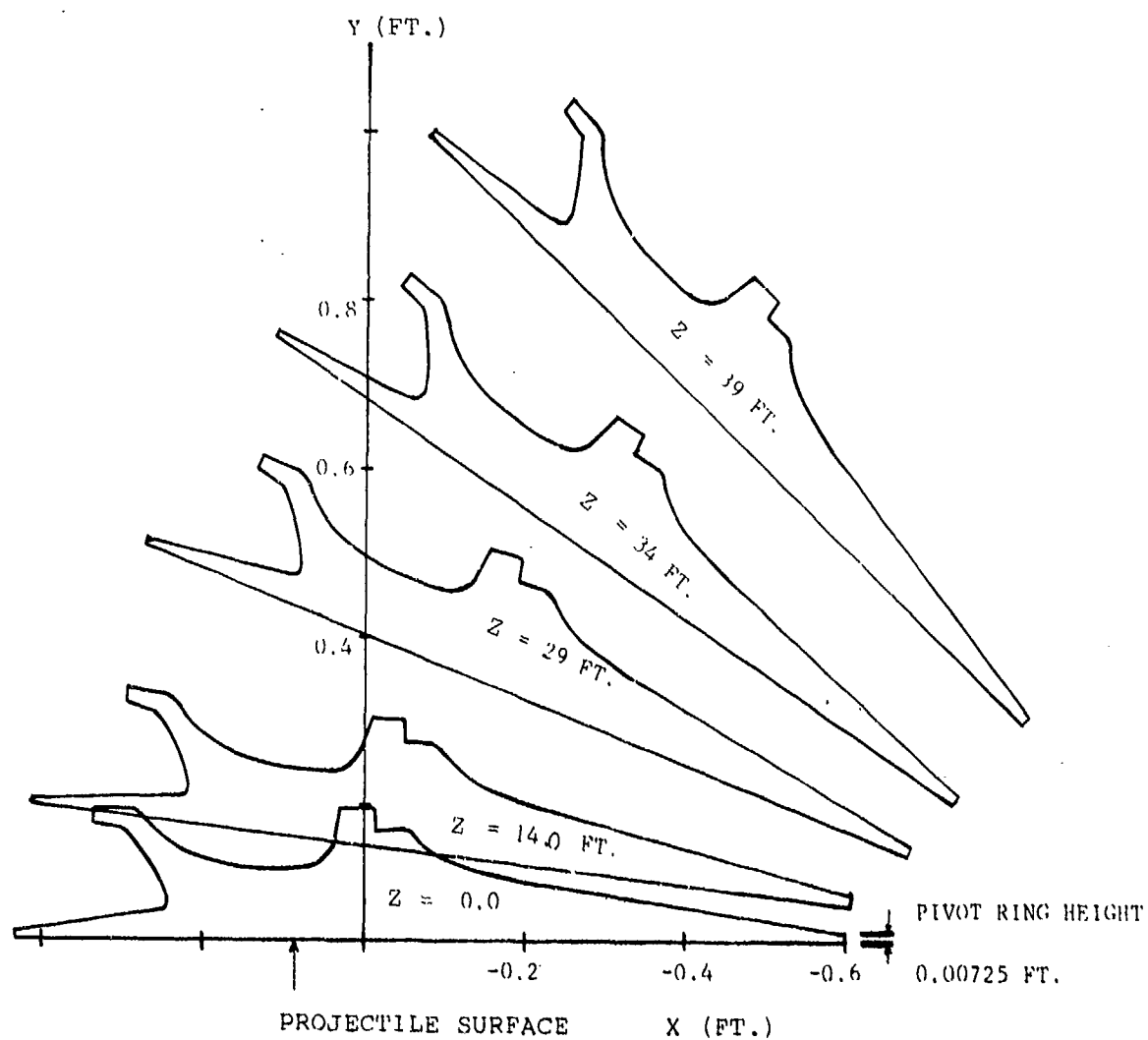
4.0 OPTIMIZATION

As noted previously, the present interaction flow model is strictly applicable only to symmetric discard situations. Furthermore, the model does not contain any procedure for evaluating interactions produced on the projectile stabilizing fins as the sabot segments sweep by. (That is, the projectile is presently modelled as a rod.) In order to use the existing tool in the design optimization mode, it was therefore necessary to define an applicable figure of merit for use in ranking the relative performance of various candidate configurations. The absolute value of the perturbing pitching moment impulse produced by a single sabot segment upon the projectile was selected as the most pertinent currently available parameter:

$$I_m = \int_0^{t_o} |Mp| \; dt \qquad (2)$$

where

$$|M_p| = |M_{p_a}| + |M_{p_m}| \qquad (3)$$

and M_{p_a} is the moment on the projectile due to aerodynamic inter-actions, M_{p_m} is the momentum on the projectile due to mechanical interactions and t_o is the time duration of the interaction process

(i.e. until the sabot bow shock is swept past the projectile trailing edge. The absolute values of the separate aerodynamic and mechanical pitching moment components have been used to represent I_m as the total possible perturbing impulsive "potential" per sabot segment. Actual perturbing pitching moments arise during discard due to sabot petal to sabot petal motion asymmetries which produce incremental aerodynamic and/or mechanical forces on the projectile surface. Optimum designs are identified herein as those having minimum values of I_m while simultaneously providing sabot segment trailing edge trajectories which do not penetrate through the projectile stabilizing fin exclusion zone.*

---

*Note that trailing edge trajectories with pivot rings are conservative since projectile slowdown is neglected.

4.1 COMPARATIVE PERFORMANCE OF 120 MM XM829 DESIGNS

Table 1 presents comparative performance results for short[9] and long[10] wheel base 120 mm XM829 sabot designs. Cases both with and without pivot rings have been computed. In addition, to these standard three segment designs, a four segment version of the short wheel base design was also considered. Figure 4 presents the corresponding sabot trailing edge trajectories (uncorrected for possible projectile slow down). The following features are noted.

Without the presence of pivot rings, all designs would suffer from unacceptibly high projectile fin impact probabilities. With the pivot rings present, the long wheel base design rotates more quickly into a high drag configuration which decelerates more rapidly off of the projectile (note lower Z_o's and I_m's of long vis-a-vis short wheel base designs). However, the mechanical inter- action component is noticed to significantly increase (by about 50%) for the long wheel base design compared to the short wheel base design (both with pivot rings). This means that any tendency toward pivot ring mechanical failure will be more of an issue for the long wheel base configuration. Encountering substantially larger mechanical forces while achieving only a small reduction in overall perturbing pitch impulse potential may not be a worthwhile design approach.

The "best" design of those considered is the four segment short wheel with pivot ring.* This design provides minimum values of I_m and flies clear of the fin exclusion zone. The primary reason for the improved performance of the four segment design is not immediately obvious since both total force (for constant pressure) and sabot mass scale linearly with surface area (i.e.: span). However, care- ful inspection of the detailed pressures and resultant dynamic motions indicated that more rapid rotation and hence deceleration occurred because the pressures acting on the spanwise outboard

---

*Note that the per segment I_m ratio is 0.69 for the 4 segment versus the 3 segment short wheeel base design with pivot rings. A ratio of 0.75 would be expected for entirely "equivalent" behaviors (based on subtend area) and this is indeed the case for the mechanical moment contributions. Also, the lower per segment value of perturbing pitch impulse potential implies less dispersive motion production during actual asymmetric discards.

-13-

	LONG WHEEL WITH PIVOT	LONG WHEEL NO PIVOT	SHORT WHEEL WITH PIVOT	SHORT WHEEL NO PIVOT	4 SEGMENT SHORT WHEEL WITH PIVOT	4 SEGMENT SHORT WHEEL NO PIVOT
MASS OF SABOT SEGMENT (SLUG x 10)	0.75197	0.75197	0.6957	0.6957	0.5240	0.5240
MOMENT OF INERTIA OF SABOT SEGMENT ABOUT C.G. (SLUG-FT^{2}x10^2)	0.2746	0.2746	0.2604	0.2604	0.1957	0.1957
$\bar{y}$ (FT)	0.6060	0.6060	0.579	0.579	0.579	0.579
$\bar{r}$ (FT)	0.08563	0.08563	0.08695	0.08695	0.0941	0.0941
Z_0 (FT)	23.4	22.0	27.8	26.8	26.9	27.1
$\int_{t}^{t_0} /M_f/dt$ (Lb-Ft-Sec)	0.9157	0.8774	1.0029	1.0538	0.6932	0.8402
$\int_{t_0} /M_\rho m/dt$ (Lb-ft-sec)	0.2030	0.1640	0.1477	0.1021	0.1106	0.0897

$\bar{y}$ = axial C.G. distance measured from trailing edge of the sabot

$\bar{r}$ = radial C.G. distance measured from the center line of the projectile

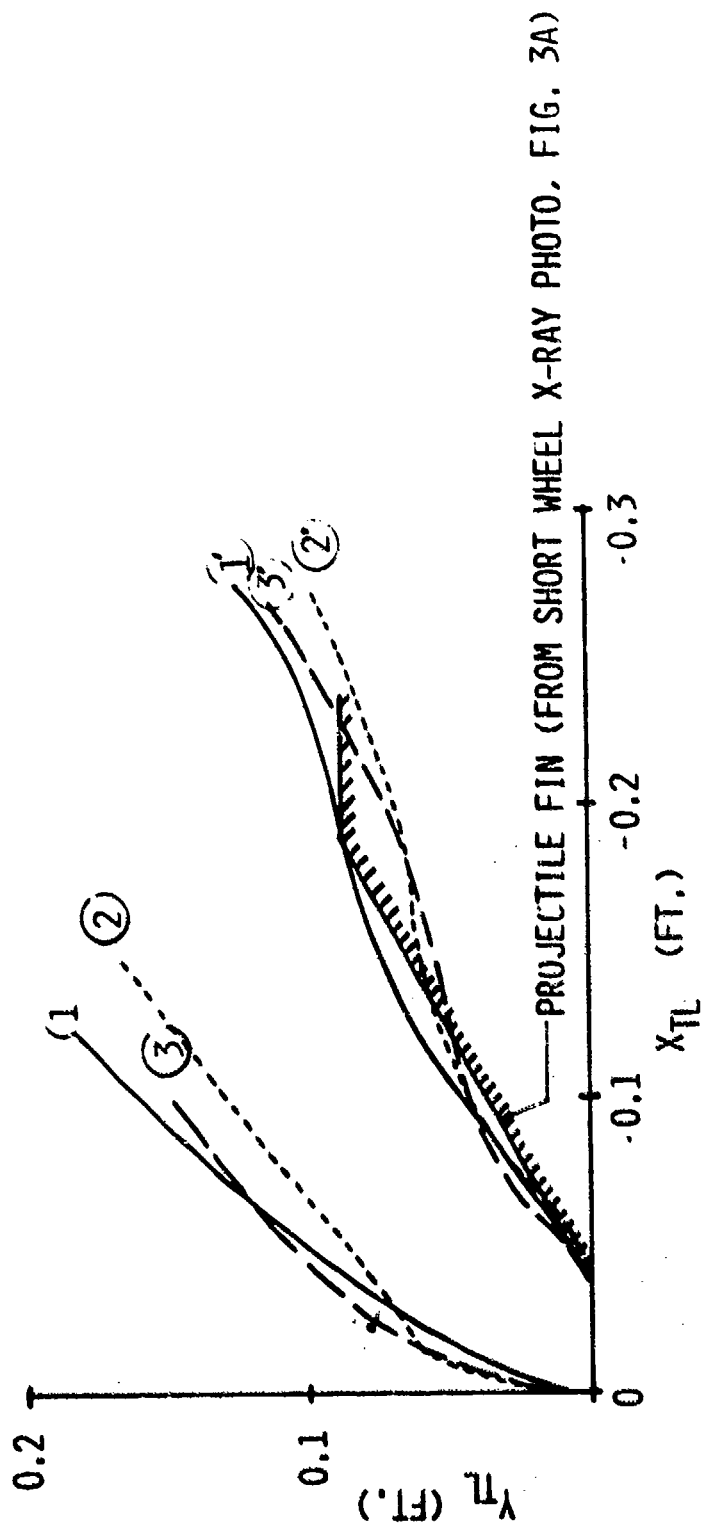FIG. 4 - XM829 SABOT TRAILING EDGE TRAJECTORIES

①' L(3) W/PVT: 3 SEGMENT LONG WHELL BASE SABOT DESIGN WITH PIVOT PING

'1' L(3) N/PVT: 3 SEGMENT LONG WHEEL BASE SABOT DESIGN NO
                    PIVOT RING

② S(3) W/PVT: ②' S(3) N/PVT

'3, S(4) W/PVT: '3' S(4) N/PVT

PROJECTILE FIN (FROM SHORT WHEEL X-RAY PHOTO. FIG. 3A)

x_{TL} (FT.)

y_{TL} (FT.)

portions of the four segment sabot scoop upper surface (bore rider)
produce larger force components in the pitch plane. This can
be visualized by drawing frontal view sketches of the two situa-
tions. The more rapid rotation also produces somewhat earlier
exit region throttling which results in some additional benefit
with regard to lift production.

4.2 DESIGN OPTIMIZATION FOR ALTERNATE 120MM XM829 CONCEPT

An alternate 120MM XM829 concept[11] was also studied.
This design was configured to shift the sabot segment center of
gravity (pivot axis) further aft toward the trailing edge in order
to reduce the magnitude of induced mechanical reaction forces
generated on the projectile and pivot ring. Comparison of
Tables 1 and 2A (for nominal D-0.16 design) shows that the mass of
this design is about the same as that of the previous short wheel
base concept, but that pitch moment of inertia is somewhat
increased while the moment arm from the trailing edge ($\overline{\xi}$) is
reduced. Both the length and position of the bore rider
were varied as shown in Table 2A. Corresponding performance
results both with and without pivot rings are shown in Table 2B
while Figure 5 presents the sabot segment trailing edge tra-
jectories. Based on these results, we conclude that the MD-0.16 de-
sign (lengthened bore rider) is "best" because it produced the
lowest levels of pitching moment impulse potential and also stays
sufficiently clear of the slender fin[12] exclusion zone to be used
without a pivot ring. For the larger fins (taken from Fig. 3A),
minimum sabot trailing edge miss distances in the fin root zone
are so small (0.02 ft.) that experimental confirmation would be
needed to resolve the pivot/no pivot issue.

Examining details of these calculations, it was found that
the MD-0.16 design lifted free sooner than other designs and then
rotated more rapidly into a high drag attitude. This is evidenced
both by the larger values of Y_{cg} for MD-0.16 at early times (i.e.:
z = 10 ft.) and the lower duration for the MD-0.16
interaction process show in Table 2B.

One other feature of these results (and those given previously
Table 1) which requires further discussion is the relative

-16-
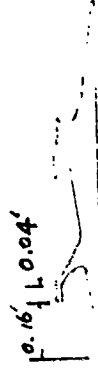
DESIGNATION	MASS (SLUG×10)	MOMENT OF INERTIA ABOUT C.G. (SLUG-FT²×10²)	$\bar{\ell}$ (FT)	$\bar{r}$ (FT)	REMARKS
D-0.00	0.7007	0.39368	0.57008	0.087725	Bore rider all the way forward
D-0.08	0.6952	0.32697	0.5547	0.08727	Bore rider half-way forward
D-0.16	0.6917	0.29399	0.54738	0.08782	Original design
MD-0.16	0.712	0.32946	0.5593	0.8965	Bore rider lengthened

-17-

TABLE 2B – ALTERNATE XM829 SABOT DESIGN (PART NO. 11834'82) PERFORMANCE*

		$\int_{t_0}$ dt (Lb-Ft-sec) ($\int_{t_0}$|Mpn|dt)	Z_0 (Ft)	@ Z_1 = 10 Ft. Pitch (deg)	XC.G.;YC.G. (Ft)	$\int_{t_1}$|Mp|dt ($\int_{t_1}$|Mpm|dt) (Lb-Ft-Sec)	@ Z_2 = 20 FT. Pitch (deg)	XC.G., YC.G. (ft.)	$\int_{t_2}$|Mp|dt (Lb-Ft-sec)	@ Z_3 = 30 FT. Pitch (deg)	XC.G.; YC.G. (ft.)	$\int_{t_3}$|Mp|dt (Lb-Ft-Sec)
D-0.00	N/PVT	0.74063 (0.1758)	22.1	1.9	0.0825;0.1473	0.58212 (0.1758)	19.0	0.2676;0.381	0.6874	48.0	0.6223;0.758	0.740625
D-0.00	W/PVT	0.785371 (0.2094)	21.6	5.9	0.0361;0.1526	0.6111 (0.2014)	23.7	0.121;0.388	0.7840	58.62	0.415;0.789	0.78531
D-0.08	N/PVT	0.811545 (0.0696)	23.7	2.7	0.0994;01351	0.4205 (0.0696)	14.2	0.265;0.317	0.7369	27.2	0.549;0.591	0.811=45
D-0.08	W/PVT	0.78862 (0.0914)	23.5	3.2	0.0483;0.141	0.43671 (0.0914)	15.7	0.134;0.3343	0.7674	30.7	0.338;0.616	0.78862
D-0.16	N/PVT	0.87449 (0.047)	25.3	2.0	0.0942;0.126	0.42519 (0.047)	11.8	0.251;0.283	0.7570	24.5	0.5156;0.535	0.87449
D-0.16	W/PVT	0.78953 (0.080)	27.3	2.5	0.0485;0.132	0.4452 (0.080)	13.1	0.128;0.304	0.7339	26.1	0.304;0.513	0.78953
MD-0.16	N/PVT	0.70375 (0.096)	19.8	4.6	0.0914;0.163	0.41613 (0.096)	21.8	0.284;0432	0.7037	52.1	0.568;0.775	0.70375
MD-0.16	W/PVT	0.63427 (0.1032)	19.8	6.7	0.0485,0.164	0.4446 (0.1032)	23.2	0.142;0.404	0.6343	52.1	0.379;0.776	0.63427

FIG. 5 - SABOT TRAILING EDGE TRAJECTORIES FOR ALTERNATE XM829 CONCEPT
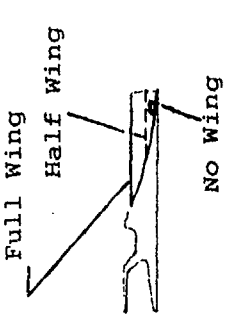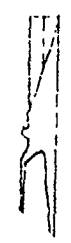
-19-
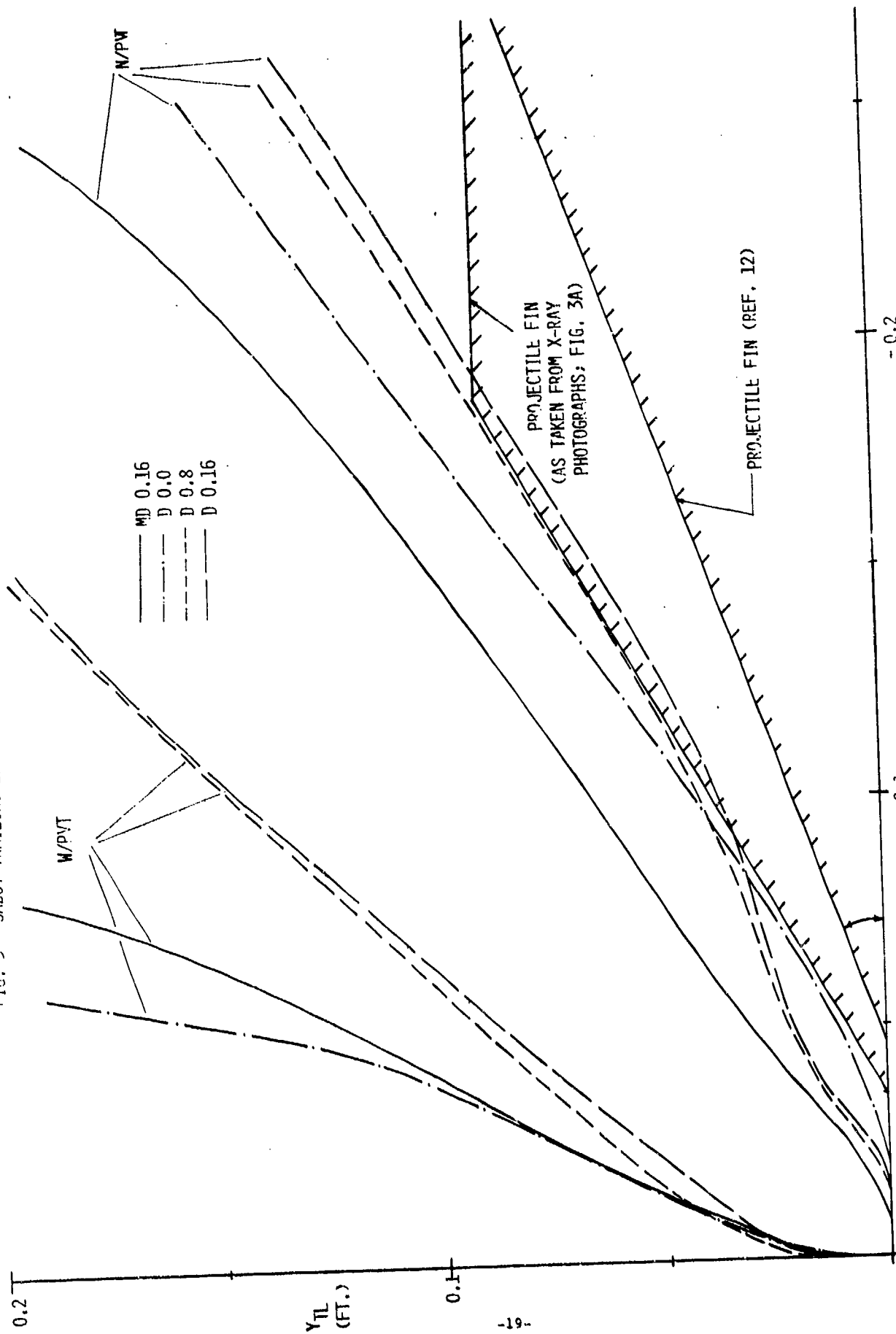
magnitude of moments computed with and without the pivot rings present. As shown in Figures 4 and 5, the primary difficulty associated with deletion of the pivot ring is the tendency to promote high probability of sabot petal impact on the projectile stabilizing fins. However, for many designs we see the interesting feature that the total pitch moment impulse with a pivot ring present is smaller than without a pivot ring, even though the mechanical interaction moment contributions are larger with the pivots present. This is true for both the three and four segment short wheel base designs given in Table 1 and for designs D-0.08, D-0.16 and MD-0.16 given in Table 2B. This behavior can be traced to the aerodynamic interaction moments late in the removal process (i.e.: note that for designs D-0.08 and D-0.16 results for I_m at Z = 20 ft. are essentially equal for pivot/no pivot cases and that mechanical interaction is over). It was found that aerodynamic moment production late in the removal process for these cases is dominated by pressures associated with outlet choking rather than those associated with the sabot bow shock impingement. Two effects then operate to produce more late time interaction moment for cases without the pivot ring present. First, at a fixed time, the axial position of the sabot is further back on the projectile for no pivot cases since the sabot axial motion is uncontrained with-out the pivot ring. This means that the relatively high pressures associated with outlet choking tend to have larger moment arms (about the projectile c.g.) for torque production. Second, the lateral motions for sabots with the pivot ring present are larger (note Y_{cg}'s for cases D-0.08 and D-0.16 at Z = 20 ft.). This results in earlier unchoking of the outlet. Thus, when the sabot with pivot present reaches the same axial station as reached by the no pivot case at an earlier time it has developed an unchoked outlet with reduced pressures and pitch moment production.

4.3 DESIGN OPTIMIZATION FOR WINGED SABOT CONCEPT

Aft mounted sabot winglets can be provided to obtain added lift by extension of the sabot segment lateral edges.[13] Table 3A presents the variations in front scoop/bore-rider geometry and winglet configuration considered. Note that all winged sabot

TABLE 3A - WINGED 120 MM XM829 SABOT DESIGN (SK480127108) GEOMETRIC PROPERTIES

	Mass (slug×10)	Moment of Inertia About C.G. (slug-Ft^2·10^2)	$\bar{x}$ (Ft)	$\bar{r}$ (Ft)	Remarks
1 - A (Full wing)	0.7230	0.3392	0.5721	0.08492	Original Drawing Full Wing
1 - B (Half wing)	0.6970	0.2960	0.5861	0.08584	Half Wing
1 - C (No wing)	0.6902	0.2799	0.5906	0.08633	No Wing
2 - A (Full wing)	0.7090	0.31413	0.5639	0.08349	As original Drawing Except Bore Rider length is reduced by 50%
2 - B (Half wing)	0.6831	0.2737	0.5783	0.08344	
2 - C (No wing)	0.6761	0.2569	0.5825	0.08480	
3 - A (Full wing)	0.7096	0.30218	0.5599	0.0845	As Original Drawing Except Bore Rider is moved backward 1/2 of the Bore rider length
3 - B (Half wing)	0.6833	0.26137	0.5737	0.0859	
3 - C		0.24613	0.5782	0.0864	

cases were computed without pivot rings present. Table 3B presents corresponding performance results while Figure 6 presents the corresponding sabot trailing edge trajectories. Based on these results, we conclude that the 3-A design is "best" because it produces somewhat lower values of pitch moment impulse potential while providing a somewhat larger minimum fin clearance (in the fin root zone) than does the next best 1-A design. Designs 1-C, 2 (A, B, C) can be eliminated because they all suffer from high probability of fin impact for the large fin case. Design 1-B also appears to provide insufficient fin clearance in the fin root zone. Design 3-C (no winglet) has small levels of clearance (about 0.01 ft.) in the mid fin zone for the large fin case. However, it appears to be a possible choice for use with the slender fin projectile design.

Careful inspection of the results indicates that we desire an initial pitching moment from the front scoop. This is needed to provide a choked flow outlet situation which produces higher pressures and more effective lift production on the winglets. Then we need to balance this scoop pitching moment (and axial force) with a counter pitch moment on the winglets for maximum lift production and rapid lateral lift off to clear the projectile fins. After we have achieved sufficient lateral velocity to ensure fin clearance, it is desirable to continue pitching up and decelerating. This occurs naturally for the winged sabot designs since as the lateral clearance of the sabot trailing edge increases, the outlet zone gap flow eventually unchokes and the winglet counter moment drops off. Note that: (i) without an effective scoop (designs 2 (ABC)) we do not achieve outlet zone choking and effective winglet lift production and (ii) without effective winglets (designs 1 (B, C)) we do not achieve sufficient early time lift for fin clearance.

Table 4 presents comparative results illustrating the performance benefits that can be obtained by using light weight advanced plastic composite materials in sabot construction. A 50% reduction in pitching moment perturbing impulse potential is achieved because identical sabot motion occurs in 50% less interaction time duration.

-22-

TABLE 3B - WINGED 120 MM XM829 SABOT DESIGN (SK480127108) PERFORMANCE*

	$\int_{to} M_f\,dt$ (lb-ft-sec) $(\int_{to}|Mpm|dt)$	z_o (FT)	@ z_1 = 10 FT.			@ z_2 = 20 FT.			@ z_3 = 30 FT.		
			Pitch θ (deg)	$X_{C.G.}$; $Y_{C.G.}$ (Ft)	$\int_{t_1}|M_f|dt$ (lb-Ft-sec) $(\int^t|Mpm|dt)$	Pitch θ (deg)	$X_{C.G.}$; $Y_{C.G.}$ (ft)	$\int_o^{t_2}|M_f|dt$ (lb-ft-sec)	Pitch θ (deg)	$X_{C.G.}$; $Y_{C.G.}$ (ft)	$\int^{t_3}|M_f|dt$ (lb-ft-sec)
1 – A	0.76170 (0.165)	19.8	4.4	0.0812;0.165	0.594 (0.165)	23.1	0.264;0.431	0.7527	59.8	0.653;0.876	0.76170
1 – B	0.70048 (0.176)	20.3	5.8	0.0695;0.165	0.604 (0.176)	23.1	0.259;0.441	0.6975	65.9	0.672;0.882	0.70481
1 – C	0.68245 (0.176)	20.2	6.9	0.0653;0.163	0.606 (0.176)	28.1	0.262;0.421	0.6824	71.2	0.722;0.875	0.68245
2 – A	0.92203 (0.0435)	25.6	1.8	0.086;0.121	0.526 (0.0435)	9.7	0.245;0.266	0.7976	22.0	0.521;0.497	0.92203
2 – B	1.00082 (0.0546)	25.2	1.8	0.073;0.121	0.5426 (0.0546)	9.8	0.239;0.263	0.8484	21.3	0.459;0.442	1.00080
2 – C	0.92946 (0.0567)	24.9	2.1	0.069;0.124	0.4837 (0.0567)	11.1	0.238;0.279	0.8132	23.0	0.525;0.516	0.92946
3 – A	0.75390 (0.0693)	21.5	3.6	0.085,0.144	0.4855 (0.0693)	15.7	0.248;0.356	0.7478	32.6	0.532;0.670	0.75391
3 – B	0.78787 (0.0715)	21.2	3.9	0.077;0.149	0.4573 (0.0715)	16.5	0.247;0.367	0.7793	32.0	0.534;0.683	0.78287
3 – C	0.75067 (0.0734)	21.5	4.0	0.073;0.151	0.4309 (0.0734)	17.8	0.246;0.374	0.7498	34.2	0.536;0.697	0.75067

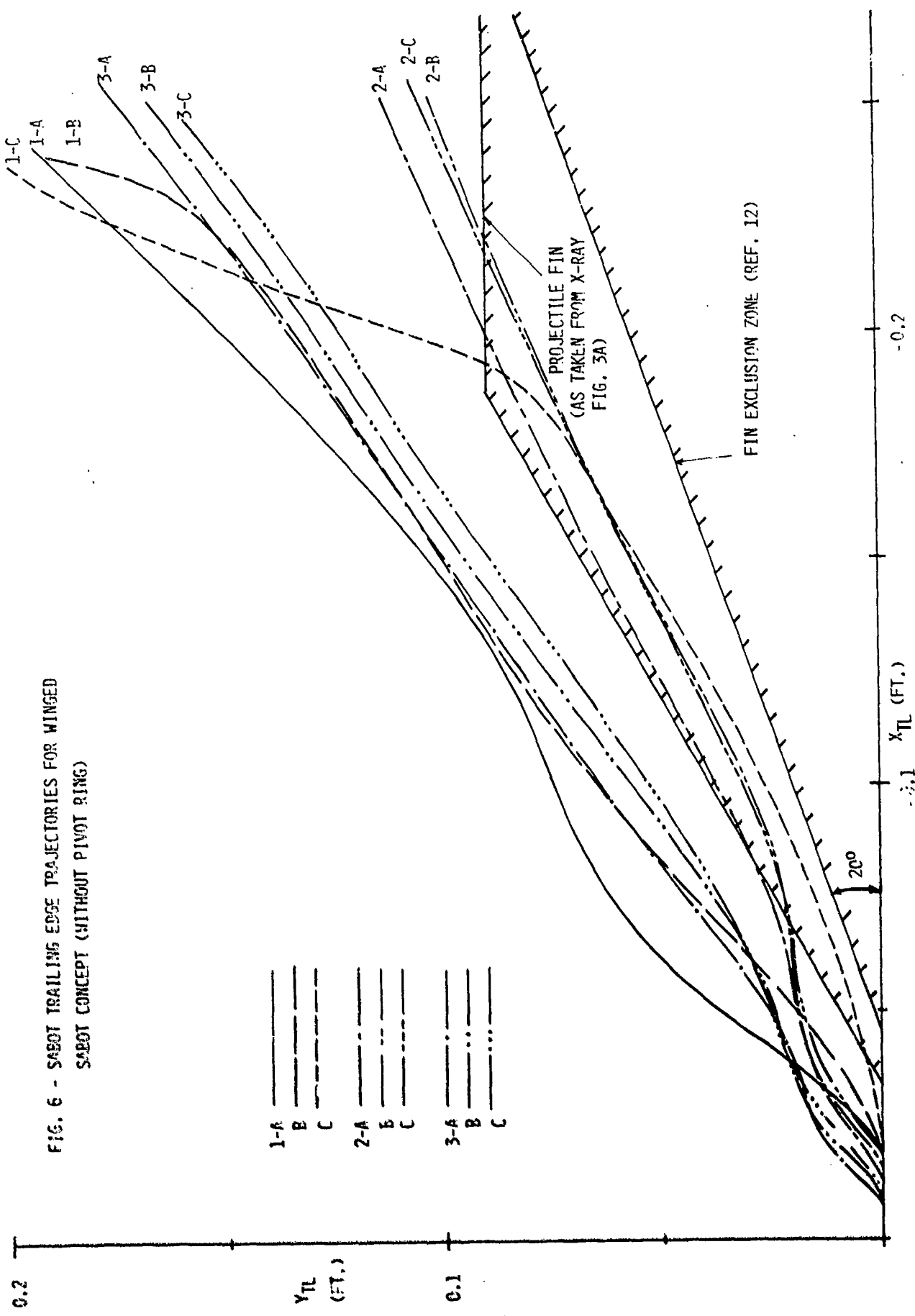FIG. 6 - SABOT TRAILING EDGE TRAJECTORIES FOR WINGED
SABOT CONCEPT (WITHOUT PIVOT RING)

-24-

TABLE 4

WEIGHT EFFECT ON SABOT PERFORMANCE

(1-A CONFIGURATION)

	$\rho = 0.05$ LB/IN^3	$\rho = 0.1$ LB/IN^3
Z_o (FT)	14.3	19.8
I_M (lb-ft-sec)	0.5256	.7617
at $Z = Z_o$: PITCHING ANGLE (DEG)	25	23
x_{TYL} (FT)	0.172	0.175
Y_{TYL} (FT)	0.119	0.127

4.4 SABOT DESIGN PRACTICES

This section summarizes the design practices which appear to result in minimum discard dynamic motion perturbations.

(i) Aft CG location - Providing a mass distribution which ocates the sabot c.g. as far aft as possible helps to minimize induced reactive forces on the projectile during the initial stages of discard where mechanical interaction forces are important.

(ii) Long/mid-positioned bore-rider - Providing a relatively long bore rider and locating it about midway back to the obturator helps to produce the most desirable pitch moment distribution. Shorter or more rearward mounted bore riders produce less pitch moment which results in less early time lift (primarily provided by outlet zone choking). The resultant motion is too axially directed, resulting in high fin impact probabilities. A long/forward mounted configuration produces too much early time pitch which causes large mechanical interaction forces. Also ·e rider location causes a stronger sabot bow shock geometry :h correspondingly high shock impingement pressures on the pro-
:tile surface. We suggest that the lower ramp always extend
>rward of the scoop face shock layer.

(iii) No Pivot Rings - The presence of pivot rings leads enhanced mechanical interaction effects. Significant ojectile slowdown can even result for cases where large axial >rce components are present. Aft mounted sabot winglets and the se of light weight sabot materials show promise for achieving ittractive pivot-ring-less designs.

(iv) Maximum Number of Sabot Segments - Using more than three sabot egments has been shown to be beneficial on a per segment basis be-
·ause bore-rider force components are more aligned with each petal's ·itch plane. Benefits also accrue on an overall basis because each segment has lower perturbing pitching moment impulse potential, nplying less capability for dispersive force production during .ctual asymmetric discard.

5.0 CONCLUSIONS AND RECOMMENDATIONS

An engineering analysis procedure which describes the sabot discard process for gun-launched projectiles has been employed to perform a sabot design optimization study. Sabot design optimization was based upon a figure of merit related to the pitching moment produced on the projectile while simultaneously precluding the possibility of sabot impact upon the projectile stabilizing fins. The use of novel winged sabot concepts and/or the use of light weight materials have been found to show promise for providing the desired sabot discard motions. Finally, design practices resulting in optimum sabot configurations have been identified.

Further development of this tool should focus upon extending the analysis capability to treat the actual asymmetric discard situation. This requires development of interaction flow modeling (perhaps based on experiments) for yawed and/or rolled sabot components and modeling applicable to sabot petal/projectile stabilizing fin interactions. Sabot performance and design optimization would then be assessed by using statistical initial condition populations (representing tip-off, roll and elastic decompression effects) to obtain statistical projectile motions in the manner currently employed to assess impact dispersion for strategic reentry systems.[14]

6.0 REFERENCES

1. Crimi, P. and Siegelman, D., "Analysis of Mechanical and Gasdynamic Loadings during Sabot Discard from Gun-Launched Projectiles," BRL Contract Report No. 341, June 1977. (AD #B0200191.)

2. Schmidt, E., "Wind Tunnel Measurements of Sabot Discard Aerodynamics," Technical Report ARBRL-TR-02246, July 1980. (AD #A088900)

3. Schmidt, E., "Wind Tunnel Measurements of Sabot Discard Aerodynamics," AIAA Paper No. 80-0429, March 1980.

4. Siegelman, D. and Crimi, P., "Projectile/Sabot Discard Aerodynamics," Contract Report ARBRL-CR-00410, December 1979. (AD #A080538)

5. Siegelman, D., Crimi, P. and Schmidt, E., "Projectile/Sabot Discard Aerodynamics," AIAA Paper No. 80-1588, August 1980.

6. Katzen, E. and Kaatari, G., "Inviscid Hypersonic Flow Around Blunt Bodies," AIAA J., Vol. 3, No. 7, pgs. 1230-1237, July 1965.

7. Boison, J. and Curtiss, H., "An Experimental Investigation of Blunt Body Stagnation Point Velocity Gradient," ARS J., pp. 130 - 135, Feb. 1959.

. Thomke, G. and Roshko, A., "Incipient Separation of a Turbulent Boundary Layer at High Reynolds Number in Two-Dimensional Supersonic Flow over a Compression Corner," NASA DAC-59819, Jan. 1969.

). BRL Drawing Number SK360127106, March 28, 1979.

. BRL Drawing Number SK360127107, April 4, 1979.

t. BRL Drawing Number 11834182, March 21, 1980.

12. Schmidt, E., Private Communication.

13. BRL Drawing Number SK480127108, April 5, 1979.

4 Siegelman, D. and Hines, R., "An Approximate Analysis of Roll/Trim Dispersion," J. Spacecraft and Rockets, Vol. 16, No. 1, pp. 15-19, Jan. - Feb. 1979.

DISTRIBUTION LIST

No. of Copies	Organization	No. of Copies	Organization
12	Commander Defense Technical Info Ctr ATTN: DDC-DDA Cameron Station Alexandria, VA 22314	6	Commander US Army Armament Research and Development Command ATTN: DRDAR-TSS (2 cys) DRDAR-TDS, Mr. Lindner DRDAR-TDA, Mr. Blick DRDAR-LC-F, Mr. A. Loeb Mr. E. Friedman Dover, NJ 07801
1	Director Defense Nuclear Agency Washington, DC 20305		
2	HQDA (DAMA-WSA, MAJ Csoka: DAMA-CSM, LTC Germann) Pentagon Washington, DC 20310	6	Commander US Army Armament Research and Development Command ATTN: DRDAR-LCV, (Mr. Reisman) DRDAR-SCN, (Mr. Kahn) DRDAR-SCW, (Mr. Townsend) DRDAR-LC, (Dr. Frasier) DRDAR-SG, (Dr. T. Hung) DRDAR-LCT (Dr. Candland) Dover, NJ 07801
1	Director US Army BMD Advanced Technology Center P.O. Box 1500, West Station Huntsville, AL 35807		
1	Commander US Army Ballistic Missile Defense Systems Command Huntsville, AL 35804	1	Commander US Army Armament Materiel Readiness Command ATTN: DRSAR-LEP-L, Tech Lib Rock Island, IL 61299
1	ODCSI, USAREUR & 7A ATTN: AEAGB-PDN (S&E) APO NY 09403		
		6	Commander US Army Watervliet Arsenal ATTN: DRDAR-LCB-TL Mr. W. Dock Dr. G. Carofano Mr. P. Alto DRDAR-LCB, Mr. T. Allen Mr. R. Billington Watervliet, NY 12189
1	Commander US Army Materiel Development and Readiness Command ATTN: DRCDMD-ST 5001 Eisenhower Avenue Alexandria, VA 22333		
1	Commander US Army Materiel Development and Readiness Command ATTN: DRCDL 5001 Eisenhower Avenue Alexandria, VA 22333	3	Commander US Army Aviation Research and Development Command ATTN: DRSAV-E DRCPM-AAH Product Manager, AH-1 P.O. Box 209 St. Louis, MO 63166

DISTRIBUTION LIST

No. of Copies	Organization	No. of Copies	Organization
1	Director US Army Air Mobility Research and Development Laboratory Ames Research Center Moffett Field, CA 94035	1	Commander US Army Materiels and Mechanics Research Center ATTN: DRXMR-ATL Watertown, MA 02172
1	Commander US Army Communications Rsch and Development Command ATTN: DRDCO-PPA-SA Fort Monmouth, NJ 07703	1	Commander US Army Research Office ATTN: CRD-AA-EH P.O. Box 12211 Research Triangle Park NC 27709
1	Commander US Army Electronics Research and Development Command Technical Support Activity ATTN: DELSD-L Fort Monmouth, NJ 07703	2	Director US Army TRADOC Systems Analysis Activity ATTN: ATAA-SL, Tech Lib ATAA-S White Sands Missile Range, NM 88002
4	Commander US Army Missile Command ATTN: DRSMI-R DRSMI-RBL DRSMI-RDK DRSMI-YDL Redstone Arsenal, AL 35809	3	Commander Naval Air Systems Command ATTN: AIR-604 Washington, DC 20360
1	Commander US Army Natick Research and Development Command ATTN: DRXRE, Dr. D. Sieling Natick, MA 01762	3	Commander Naval Ordnance Systems Cmd ATTN: ORD-9132 Washington, DC 20360
1	Commander US Army Tank Automotive Research & Development Cmd ATTN: DRDTA-UL Warren, MI 48090	2	Commander David W. Taylor Naval Ship Research & Development Center ATTN: Lib Div, Code 522 Aerodynamic Lab Bethesda, MD 20084
1	Commander US Army Jefferson Proving Ground ATTN: STEJP-TD-D Madison, IN 47250	3	Commander Naval Surface Weapons Center ATTN: Code 6X Mr. F.H. Maille Dr. J. Yagla Dr. G. Moore Dahlgren, VA 22448

No. of Copies	Organization	No. of Copies	Organization
1	Commander Naval Surface Weapons Center ATTN: Code 730, Tech Lib Silver Spring, MD 20910	1	Director National Aeronautics and Space Administration Langley Research Center ATTN: MS 185, Tech Lib Langley Station Hampton, VA 23365
1	Commander Naval Weapons Center ATTN: Code 553, Tech Lib China Lake, CA 93555	1	Director NASA Scientific & Technical Information Facility ATTN: SAK/DL P.O. Box 8757 Baltimore/Washington International Airport, MD 21240
1	Commander Naval Research Laboratory ATTN: Tech Info Div Washington, DC 20375		
1	Commander Naval Ordnance Station ATTN: Code FS13A, P. Sewell Indian Head, MD 20640	1	AAI Corporation ATTN: Dr. T. Stastny Cockeysville, MD 21030
1	AFRPL/LKCB, Dr. Horning Edwards AFB, CA 93523	1	Advanced Technology Labs ATTN: Dr. J. Erdos Merrick & Steward Avenue Westbury, NY 11590
2	AFATL (DLDL, Dr. D.C. Daniel; Tech Lib) Eglin AFB, FL 32542		
1	AFWL/DEV Kirtland AFB, NM 87117	1	Aerospace Corporation ATTN: Dr. T. Taylor P.O. Box 92957 Los Angeles, CA 90009
1	ASD/XRA (Stinfo) Wright-Patterson AFB, OH 45433	1	ARO, Inc. ATTN: Tech Lib Arnold AFS, TN 37389
1	Director National Aeronautics and Space Administration George C. Marshall Space Flight Center ATTN: MS-I, Lib Huntsville, AL 38512	1	ARO, Inc. Von Karman Gasdynamics Facility ATTN: Dr. J. Adams Arnold AFS, TN 37389
1	Director Jet Propulsion Laboratory ATTN: Tech Lib 2800 Oak Grove Drive Pasadena, CA 91103	1	ARTEC Associates, Inc. ATTN: Dr. S. Gill 26046 Eden Landing Road Hayward, CA 94545

DISTRIBUTION LIST

No. of Copies	Organization	No. of Copies	Organization
2	AVCO Associates, Inc. ATTN: Dr. W. Reinecke Dr. D. Siegelman 201 Lowell Street Wilmington, MA 01887	1	Winchester-Western Division Olin Corporation New Haven, CT 06504
1	Battelle Columbus Laboratories ATTN: J.E. Backofen, Jr. 505 King Avenue Columbus, OH 43201	1	Rockwell Int'l Science Center ATTN: Dr. Norman Malmuth P.O. Box 1085 1000 Oaks, CA 91360
1	Technical Director Colt Firearms Corporation 150 Huyshope Avenue Hartford, CT 14061	1	Sandia Laboratories ATTN: Aerodynamics Dept Org 5620, R. Maydew Albuquerque, NM 87115
1	Flow Simulations, Inc. ATTN: Dr. J. Steger 735 Alice Ave Mountain View, CA 94041	1	S&D Dynamics, Inc. ATTN: Dr. M. Soifer 755 New York Avenue Huntington, NY 11743
2	General Electric Corporation Armaments Division ATTN: Mr. R. Whyte Mr. J. MacNeil Lakeside Avenue Burlington, VT 05401	1	Guggenheim Aeronautical Lab California Institute of Tech ATTN: Tech Lib Pasadena, CA 91104
1	Honeywell, Inc. ATTN: Mail Station MN 112190 (G. Stilley) 600 Second Street, North Hopkins, MN 55343	1	Franklin Institute ATTN: Tech Lib Race & 20th Streets Philadelphia, PA 19103 Director Applied Physics Laboratory The Johns Hopkins University Johns Hopkins Road Laurel, MD 20810
1	Hughes Helicopter Company Bldg. 2, MST22B ATTN: Mr. R. Forker Centinella and Teel Streets Culver City, CA 90230	1	Massachusetts Institute of Technology Dept of Aeronautics and Astronautics ATTN: Tech Lib
1	Martin Marietta Aerospace ATTN: Mr. A.J. Culotta P.O. Box 5387 Orlando, FL 32805		77 Massachusetts Avenue Cambridge, MA 02139

No. of Copies	Organization	No. of Copies	Organization
1	Ohio State University Dept of Aeronautics and Astronautical Engineering ATTN: Tech Lib Columbus, OH 43210	1	ARO, Inc. Von Karman Gasdynamics Facility ATTN: W. Lawrence Arnold AFS, TN 37389
2	Polytechnic Institute of New York Graduate Center ATTN: Tech Lib Dr. G. Moretti Route 110 Farmingdale, NY 11735		
1	Director Forrestal Research Center Princeton University Princeton, NJ 08540		
1	Southwest Research Institute ATTN: Mr. Peter S. Westine P.O. Drawer 28510 8500 Culebra Road San Antonio, TX 78228		

Aberdeen Proving Ground

Dir, USAMSAA
  ATTN: DRXSY-D
        DRXSY-MP, H. Cohen

Cdr, USATECOM
  ATTN: DRSTE-TO-F

Cdr, USA CSL/EA
  ATTN: SAREA-DE-W
       Bldg E3516

Dir, USACSL
  Bldg. E3516, EA
  ATTN: DRDAR-CLB-PA